

HAMILTONIAN-PRESERVING DISCONTINUOUS GALERKIN METHODS FOR THE LIOUVILLE EQUATION WITH DISCONTINUOUS POTENTIAL

BOYANG YE*, SHI JIN †, YULONG XING‡, AND XINGHUI ZHONG§

Abstract. Numerically solving the Liouville equation in classical mechanics with a discontinuous potential often leads to the challenges of how to preserve the Hamiltonian across the potential barrier and a severe time step constraint according to the CFL condition. Motivated by the Hamiltonian-preserving finite volume schemes by Jin and Wen [19], we introduce a Hamiltonian-preserving discontinuous Galerkin (DG) scheme for the Liouville equation with discontinuous potential in this paper. The DG method can be designed with arbitrary order of accuracy, and offers many advantages including easy adaptivity, compact stencils and the ability of handling complicated boundary condition and interfaces. We propose to carefully design the numerical fluxes of the DG methods to build the behavior of a classical particle at the potential barrier into the numerical scheme, which ensures the continuity of the Hamiltonian across the potential barrier and the correct transmission and reflection condition. Our scheme is proved to be positive and stable in L^1 norm if the positivity-preserving limiter is applied. Numerical examples are provided to illustrate the accuracy and effectiveness of the proposed numerical scheme.

Key words. discontinuous Galerkin method; Liouville equation; Hamiltonian-preserving; discontinuous potential; boundary-preserving limiter

AMS subject classifications. 65M60, 35L45, 70H99

1. Introduction. In this paper, we develop and analyze high order Hamiltonian-preserving discontinuous Galerkin (DG) methods for the d -dimensional Liouville equation in classical mechanics

$$(1.1) \quad f_t + \nabla_{\mathbf{v}} H \cdot \nabla_{\mathbf{x}} f - \nabla_{\mathbf{x}} H \cdot \nabla_{\mathbf{v}} f = 0, \quad \mathbf{x}, \mathbf{v} \in \mathbb{R}^d,$$

where the Hamiltonian H is given by

$$(1.2) \quad H = \frac{1}{2} |\mathbf{v}|^2 + V(\mathbf{x}),$$

and $V(\mathbf{x})$ is the potential. Here $f(t, \mathbf{x}, \mathbf{v})$ is the probability density function of particles at position \mathbf{x} , time t and traveling with velocity \mathbf{v} . The Liouville equation (1.1) can be viewed as a different Eulerian formulation of Newton's second law:

$$\frac{d\mathbf{x}}{dt} = \mathbf{v}, \quad \frac{d\mathbf{v}}{dt} = -\nabla_{\mathbf{x}} V,$$

which is a Hamiltonian system with the Hamiltonian H defined in (1.2).

If the potential $V(x)$ is smooth, the Liouville equation (1.1) is a linear kinetic equation, which has been well studied in the literature. Many existing numerical methods can be applied to provide good numerical approximation. However, a discontinuous potential $V(x)$ may cause extra challenges both theoretically and numerically, and special attention shall be paid to the case with a potential barrier when the potential $V(x)$ is discontinuous. Potential barriers appear in many practical physical problems including the quantum tunneling, materials or media with interfaces, etc. Under such case, the Liouville equation (1.1) becomes a linear hyperbolic model with measure-valued coefficients. We refer to the results in [1, 2, 3, 12, 16, 27, 28] for some theoretical analysis on the uniqueness of weak solutions to transport equation with discontinuous (but not measure-valued) coefficients, as the latter can be viewed as a special case of the Liouville equation. Numerically, standard numerical methods may suffer from two challenges [19]. First, numerical approximation of V_x near the discontinuity is of the order $O(1/\Delta x)$, therefore, if an explicit numerical method is used for time discretization, the stringent CFL condition $\Delta t = O(\Delta x \Delta v)$ is required, with $\Delta x, \Delta v$ being the mesh size under the one-dimensional spatial space and one-dimensional velocity space (1D1V) setting. This leads to smaller

* School of Mathematical Sciences, Zhejiang University, Hangzhou, Zhejiang 310058, P.R. China. 11935020@zju.edu.cn

† School of Mathematical Sciences, Institute of Natural Sciences, MOE-LSC, Shanghai Jiao Tong University, Shanghai, Shanghai 200240, P.R. China. shijin-m@sjtu.edu.cn

‡ Department of Mathematics, The Ohio State University, Columbus, OH 43210, USA. xing.205@osu.edu

§ School of Mathematical Sciences, Zhejiang University, Hangzhou, Zhejiang 310058, P.R. China. zhongxh@zju.edu.cn

37 Δt , hence more expensive computation. Second, the Hamiltonian $H = \xi^2/2 + V(x)$ is not preserved across the
 38 discontinuities of $V(x)$, which may lead to at least a poor numerical resolution, or more seriously, unphysical
 39 solutions [21].

It is well-known from classical mechanics that, across a potential barrier, the Hamiltonian should remain constant. Motivated by this, Hamiltonian-preserving methods have been proposed and studied in [19] to solve the Liouville equation with discontinuous potential based on finite difference and finite volume approaches. The main idea was to use the behavior of the classical particle at the potential barrier, namely, transmission or reflection, and build it into the design of the Hamiltonian-preserving methods to be consistent with the constant Hamiltonian across the discontinuity. This mechanism was first used to construct the numerical flux and to build the well-balanced kinetic scheme in [26] for the shallow water equations with non-flat topography, in order to preserve the steady state solution. It was also shown in [19] that the proposed explicit Hamiltonian-preserving schemes admit a standard CFL condition $\Delta t = O(\Delta x, \Delta v)$, and the positivity property and the stability in L^1 and L^∞ norms are also provided. The proof of the L^1 -stability and error estimates of the proposed schemes are further discussed in [34, 35, 33, 23]. We also refer readers to [20, 21] for the Hamiltonian-preserving methods to solve the Liouville equation (1.1) arising from the applications in geometrical optics, with the Hamiltonian

$$H = c(\mathbf{x})|\mathbf{v}|,$$

where $c(\mathbf{x})$ is the local wave speed of the medium. It can be viewed as the high frequency limit of the second order wave equation

$$u_{tt} - c(\mathbf{x})^2 \Delta u = 0, \quad t > 0, \quad \mathbf{x} \in \mathbb{R}^d.$$

40 Here the wave speed $c(\mathbf{x})$ has isolated discontinuities due to different media, and waves crossing the discontinuous
 41 interface will be transmitted or reflected. Hamiltonian-preserving methods for more complex cases like
 42 high frequency waves propagating through different media can be found in [17, 22, 32].

43 In this paper, we consider solving the Liouville equation (1.1) in the discontinuous Galerkin (DG) frame-
 44 work. DG methods are a class of finite element methods, where both the numerical solution and the test
 45 functions belong to discontinuous piecewise polynomial spaces. They were first designed to solve linear trans-
 46 port equations in [30], and later were extended to solve hyperbolic conservation laws in a series of papers
 47 [7, 8, 9, 10]. DG methods have been successfully applied to a wide range of mathematical models, including
 48 the kinetic equations, see [6, 13, 15, 29, 4, 5] and the references therein for an incomplete list.

49 DG methods enjoy many advantages, including h-p adaptivity, arbitrarily unstructured meshes, compact
 50 stencils, efficient parallel implementation, and the ability of handling complicated boundary conditions and
 51 curved interface, etc. The goal of this paper is to design Hamiltonian-preserving DG (HPDG) methods for
 52 the Liouville equation (1.1), extending the low order Hamiltonian-preserving finite difference and finite volume
 53 methods in [19] to high order HPDG methods. As illustrated in [19], one of the key ideas to design Hamiltonian-
 54 preserving methods is to build the behavior of a classical particle at the potential barrier into the numerical
 55 scheme. Here, we propose to carefully design the numerical fluxes of the DG methods to adopt such mechanism.
 56 The HPDG method is built upon the standard DG method for hyperbolic conservation laws, with extra
 57 attention paid to the design of numerical fluxes at the positions where the potential $V(x)$ is discontinuous to
 58 ensure the continuity of the Hamiltonian across the potential barrier. As a result, the boundary integration of
 59 numerical fluxes at the cell interfaces may be converted into another integration over a range of cell interfaces,
 60 which can be evaluated numerically via a carefully designed Gaussian quadrature rule. In [19], the low order
 61 Hamiltonian-preserving finite difference and finite volume methods were proven to be positive and stable in L^1
 62 and L^∞ norm. After extending these to arbitrary high order HPDG methods, one non-trivial challenge lies in
 63 the stability of the resulting method. To provide extra robustness and stability, a simple positivity-preserving
 64 limiter, studied in [36] for DG methods, is combined with the proposed HPDG methods. We demonstrate
 65 theoretically that the resulting DG methods preserve the non-negativity of the numerical solution, and have
 66 the L^1 stability, even under the situation when the potential $V(x)$ is discontinuous. Numerical examples are
 67 provided for both one-dimensional (1D1V) and two-dimensional (2D2V) Liouville equations to demonstrate
 68 the performance of the proposed methods.

69 The paper is organized as follows: In Section 2, we first discuss the problems with the standard DG
 70 method to solve the Liouville equation under 1D1V setting with discontinuous potentials. We then present the

71 Hamiltonian-preserving numerical fluxes by adopting the behavior of classical particles at a potential barrier.
 72 This leads to the HPDG methods. In addition, we combine the resulting method with a simple positivity-
 73 preserving limiter to ensure the solution stay non-negative during the simulation. In Section 3, we establish the
 74 positivity and stability analysis for our Hamiltonian-preserving scheme. We extend the proposed methods to
 75 two-dimensional space in Section 4. In Section 5, several numerical examples are presented to investigate the
 76 accuracy and effectiveness of our Hamiltonian-preserving scheme. We conclude the paper with some remarks
 77 in Section 6.

78 **2. Hamiltonian-preserving DG methods.** In this section, we lay out the details of the algorithm
 79 formulation of the HPDG method for the Liouville equation (1.1) under the1DIV setting, given by

$$80 \quad (2.1) \quad f_t + \xi f_x - V_x f_\xi = 0,$$

82 equipped with suitable initial and boundary conditions, where ξ denotes the one-dimensional variable in the \mathbf{v}
 83 direction. Our starting point is the standard DG method presented in the following section.

84 **2.1. Standard DG methods.** In this section, we briefly present the standard DG method for solving
 85 (2.1) and discuss the difficulties arising from the discontinuous potentials.

86 We first introduce some notations. Assume $x \in [-L, L]$ and $\xi \in [-A_c, A_c]$. The domain is uniformly (to
 87 simplify the presentation) partitioned as follows:

$$88 \quad -L = x_{\frac{1}{2}} < x_{\frac{3}{2}} < \cdots < x_{N_x + \frac{1}{2}} = L, \quad -A_c = \xi_{\frac{1}{2}} < \xi_{\frac{3}{2}} < \cdots < \xi_{N_\xi + \frac{1}{2}} = A_c.$$

89 We use a mesh that is a tensor product of grids in the x and ξ direction, respectively, defined as

$$90 \quad K_{ij} = [x_{i-\frac{1}{2}}, x_{i+\frac{1}{2}}] \times [\xi_{j-\frac{1}{2}}, \xi_{j+\frac{1}{2}}], \quad I_i = [x_{i-\frac{1}{2}}, x_{i+\frac{1}{2}}], \quad J_j = [\xi_{j-\frac{1}{2}}, \xi_{j+\frac{1}{2}}].$$

Denote the cell center as $x_i = \frac{1}{2}(x_{i+\frac{1}{2}} + x_{i-\frac{1}{2}})$ and $\xi_j = \frac{1}{2}(\xi_{j+\frac{1}{2}} + \xi_{j-\frac{1}{2}})$. Denote the mesh size as $\Delta x =$
 $x_{i+\frac{1}{2}} - x_{i-\frac{1}{2}}$ and $\Delta \xi = \xi_{j+\frac{1}{2}} - \xi_{j-\frac{1}{2}}$. We also define a discontinuous Galerkin finite element approximation
 space as

$$\mathbb{V}_h^k := \{v : v|_{K_{ij}} \in P^k(K_{ij}), \quad 1 \leq i \leq N_x, \quad 1 \leq j \leq N_\xi\},$$

92 where $P^k(K_{ij})$ denotes the set of polynomials of total degree up to k on cell K_{ij} . Denote v^-, v^+ as the left
 93 and right limits of the function v at the cell interface, respectively. We also introduce the following notations
 94 to simplify the presentation:

$$95 \quad (2.2) \quad (u, v)_{K_{ij}} = \int_{K_{ij}} uv \, dx d\xi, \quad \langle u, v \rangle_{I_i} = \int_{I_i} uv \, dx, \quad \langle u, v \rangle_{J_j} = \int_{J_j} uv \, d\xi.$$

97 With a slight abuse of notation, the standard semi-discrete DG method for solving (2.1) is defined as
 98 follows: to find a unique function $f : [0, T] \rightarrow \mathbb{V}_h^k$, such that: for $i = 1, \dots, N_x, j = 1, \dots, N_\xi$,

$$99 \quad (2.3) \quad (f_t, \phi)_{K_{ij}} - (\xi f, \phi_x)_{K_{ij}} + \left\langle \xi \hat{f}_{i+\frac{1}{2}, \xi}, \phi(x_{i+\frac{1}{2}}^-, \xi) \right\rangle_{J_j} - \left\langle \xi \hat{f}_{i-\frac{1}{2}, \xi}, \phi(x_{i-\frac{1}{2}}^+, \xi) \right\rangle_{J_j} \\
 100 \quad + (V_x f, \phi_\xi)_{K_{ij}} - \left\langle V_x \tilde{f}_{x, j+\frac{1}{2}}, \phi(x, \xi_{j+\frac{1}{2}}^-) \right\rangle_{I_i} + \left\langle V_x \tilde{f}_{x, j-\frac{1}{2}}, \phi(x, \xi_{j-\frac{1}{2}}^+) \right\rangle_{I_i} = 0,$$

101 holds for all test functions $\phi \in \mathbb{V}_h^k$. Here

$$102 \quad (2.4) \quad \hat{f}_{i+\frac{1}{2}, \xi} = \hat{f}(x_{i+\frac{1}{2}}, \xi), \quad \tilde{f}_{x, j+\frac{1}{2}} = \tilde{f}(x, \xi_{j+\frac{1}{2}})$$

104 are the so-called numerical fluxes, defined at the cell interfaces and in general depend on the values of the
 105 numerical solution f from both sides of the interface. They are usually taken as monotone fluxes and we refer

106 the readers to the review paper [11] for more details. For example, we can take the following simple upwind
 107 numerical fluxes

$$108 \quad (2.5) \quad \hat{f}_{i+\frac{1}{2},\xi} = \begin{cases} f(x_{i+\frac{1}{2}}^-, \xi) & \text{if } \xi \geq 0, \\ f(x_{i+\frac{1}{2}}^+, \xi) & \text{if } \xi < 0, \end{cases}$$

$$109 \quad (2.6) \quad \tilde{f}_{x,j+\frac{1}{2}} = \begin{cases} f(x, \xi_{j+\frac{1}{2}}^+) & \text{if } V_x \geq 0, \\ f(x, \xi_{j+\frac{1}{2}}^-) & \text{if } V_x < 0. \end{cases}$$

111 Thus we obtain a standard semi-discrete DG scheme for solving the Liouville equation (2.1).

112 For the temporal discretization, we consider the third-order strong-stability-preserving (SSP) Runge-Kutta
 113 (RK) method [31]. For solving

$$114 \quad (2.7) \quad \frac{du}{dt} = \mathcal{L}(u).$$

115 with \mathcal{L} being a spatial discretization operator, the SSP-RK method is given by

$$116 \quad (2.8) \quad \begin{aligned} u^{(1)} &= u^n + \Delta t \mathcal{L}(u^n), \\ u^{(2)} &= \frac{3}{4}u^n + \frac{1}{4} \left(u^{(1)} + \Delta t \mathcal{L}(u^{(1)}) \right), \\ u^{n+1} &= \frac{1}{3}u^n + \frac{2}{3} \left(u^{(2)} + \Delta t \mathcal{L}(u^{(2)}) \right). \end{aligned}$$

117
 118 The standard DG method (2.3), combined with the SSP-RK temporal discretization (2.8), works very well
 119 when the potential $V(x)$ is smooth. However, if $V(x)$ contains discontinuity, the standard DG method suffers
 120 from the following two difficulties as outlined in [19]:

- 121 • The Hamiltonian $H = \xi^2/2 + V(x)$ is not preserved across the discontinuities of $V(x)$, which may lead
 122 to an unphysical solution or poor numerical resolution.
- 123 • The CFL condition of the DG scheme, coupled with an explicit time discretization, is given by

$$124 \quad (2.9) \quad \Delta t \left[\frac{\max_j |\xi_j|}{\Delta x} + \frac{\max_i |V_x|_i}{\Delta \xi} \right] \leq CFL,$$

125
 126 where $|V_x|_i$ denotes some numerical approximation of V_x at $x = x_i$. Usually, to have a stable approxi-
 127 mation, the time step needs to satisfy $\Delta t \leq O(\Delta x, \Delta \xi)$, for smooth potentials $V(x)$. For discontinuous
 128 potential V_x , we have $\max |V_x|_i = O(1/\Delta x)$ in the numerical approximation if one smooths V_x through
 129 a few mesh points, which leads to a more stringent and unnecessary CFL condition $\Delta t \leq O(\Delta x \Delta \xi)$.

130 **2.2. Hamiltonian-preserving numerical flux.** To overcome these numerical difficulties, in this section,
 131 we unravel the reconstruction of the Hamiltonian-preserving numerical flux for the DG method for solving the
 132 Liouville equation with a discontinuous potential, based on the behavior of a classical particle at a potential
 133 barrier.

134 By the theory of the classical mechanics, a particle at a potential barrier either crosses it with a different
 135 momentum or is reflected, depending on its momentum and the strength of the potential barrier. Across the
 136 potential barrier, the Hamiltonian $H = \xi^2/2 + V(x)$ should be preserved, i.e.,

$$137 \quad (2.10) \quad \frac{1}{2}(\xi^-)^2 + V^- = \frac{1}{2}(\xi^+)^2 + V^+,$$

138
 139 where the superscript \pm denote the right and left limits of the function at the potential barrier. Therefore, at
 140 the discontinuity of the potential $V(x)$, given the velocity ξ^- on the left of the discontinuity, the velocity ξ^+
 141 on the right can be computed by this constant Hamiltonian condition, yielding

$$142 \quad (2.11) \quad \xi^+ = \begin{cases} \sqrt{(\xi^-)^2 + 2(V^- - V^+)} & \text{if } (\xi^-)^2 + 2(V^- - V^+) \geq 0, \\ -\xi^- & \text{otherwise.} \end{cases}$$

144 More details to explain the behavior of a classical particle at a potential barrier can be found in [19]. We
 145 remark here that in defining numerical fluxes, we use the property that the density function $f(t, x, \xi)$ stays
 146 unchanged across the discontinuity of the potential, in the following manner:

$$147 \quad (2.12) \quad f(t, x^-, \xi^-) = f(t, x^+, \xi^+),$$

149 where x is some discontinuous point of $V(x)$, and ξ^\pm are related by (2.11).

150 Now we use the above mechanism to construct Hamiltonian-preserving numerical flux of high-order DG
 151 methods for solving (2.1), in order to maintain a constant Hamiltonian across the potential barrier. Throughout
 152 this paper, we assume that the discontinuous points of the potential $V(x)$ are located at the cell interface
 153 and $V(x)$ is Lipschitz continuous in the region between these discontinuities. In order to take care of the
 154 discontinuity of the potential, we first introduce numerical fluxes $\hat{f}_{i-\frac{1}{2}, \xi}^+, \hat{f}_{i+\frac{1}{2}, \xi}^-$ at each cell interface in the
 155 x -direction and modify the semi-discrete DG scheme (2.3) as

$$156 \quad (2.13) \quad \begin{aligned} & (f_t, \phi)_{K_{ij}} - (\xi f, \phi_x)_{K_{ij}} + \left\langle \xi \hat{f}_{i+\frac{1}{2}, \xi}^-, \phi(x_{i+\frac{1}{2}}^-, \xi) \right\rangle_{J_j} - \left\langle \xi \hat{f}_{i-\frac{1}{2}, \xi}^+, \phi(x_{i-\frac{1}{2}}^+, \xi) \right\rangle_{J_j} \\ & + (V_x f, \phi_\xi)_{K_{ij}} - \left\langle V_x \tilde{f}_{x, j+\frac{1}{2}}, \phi(x, \xi_{j+\frac{1}{2}}^-) \right\rangle_{I_i} + \left\langle V_x \tilde{f}_{x, j-\frac{1}{2}}, \phi(x, \xi_{j-\frac{1}{2}}^+) \right\rangle_{I_i} = 0, \end{aligned}$$

158 where the numerical fluxes $\tilde{f}_{x, j \pm \frac{1}{2}}$ in the ξ direction still take the form of upwind fluxes defined in (2.6). Note
 159 that if $V(x)$ is continuous at the point $x_{i-\frac{1}{2}}$, both $\hat{f}_{i-\frac{1}{2}, \xi}^+$ and $\hat{f}_{i-\frac{1}{2}, \xi}^-$ reduce to the standard numerical fluxes
 160 $\hat{f}_{i+\frac{1}{2}, \xi}$ as defined earlier.

161 Now, assume $V(x)$ is discontinuous at $x_{i-\frac{1}{2}}$, our focus is on the reconstruction of the numerical fluxes
 162 $\hat{f}_{i-\frac{1}{2}, \xi}^\pm$ in the scheme (2.13), which is explained in details in the following.

163 If $\xi > 0$, following the idea of upwind flux, we define

$$164 \quad (2.14) \quad \hat{f}_{i-\frac{1}{2}, \xi}^- = f(x_{i-\frac{1}{2}}^-, \xi),$$

166 which is the same as the standard upwind flux in (2.5) and ξ is taken from the interior of the cell. But for the
 167 other flux $\hat{f}_{i-\frac{1}{2}, \xi}^+$, we define it as

$$168 \quad (2.15) \quad \hat{f}_{i-\frac{1}{2}, \xi}^+ = f(x_{i-\frac{1}{2}}^-, \tilde{\xi}),$$

170 where $\tilde{\xi}$ is connected to ξ via the relation (2.10), i.e.,

$$171 \quad (2.16) \quad \frac{1}{2} \tilde{\xi}^2 + V(x_{i-\frac{1}{2}}^-) = \frac{1}{2} \xi^2 + V(x_{i-\frac{1}{2}}^+),$$

173 or the equivalent form (2.11):

$$174 \quad (2.17) \quad \tilde{\xi} = \begin{cases} \sqrt{\xi^2 - 2(V(x_{i-\frac{1}{2}}^-) - V(x_{i-\frac{1}{2}}^+))} & \text{if } \xi^2 - 2(V(x_{i-\frac{1}{2}}^-) - V(x_{i-\frac{1}{2}}^+)) \geq 0, \\ -\xi & \text{otherwise.} \end{cases}$$

176 The definition of the flux (2.15) is consistent with the upwind flux (2.5) when $V(x)$ is continuous, since
 177 $V(x_{i-\frac{1}{2}}^-) = V(x_{i-\frac{1}{2}}^+)$ under such case and we have $\tilde{\xi} = \xi$.

178 If $\xi < 0$, we similarly define

$$179 \quad (2.18) \quad \hat{f}_{i-\frac{1}{2}, \xi}^+ = f(x_{i-\frac{1}{2}}^+, \xi),$$

181 following the upwind flux (2.5), and

$$182 \quad (2.19) \quad \hat{f}_{i-\frac{1}{2}, \xi}^- = f(x_{i-\frac{1}{2}}^+, \tilde{\xi}),$$

184 where $\tilde{\xi}$ is again connected to ξ via the relation (2.10) or (2.11), i.e.,

$$185 \quad (2.20) \quad \tilde{\xi} = \begin{cases} -\sqrt{\xi^2 + 2(V(x_{i-\frac{1}{2}}^-) - V(x_{i-\frac{1}{2}}^+))} & \text{if } \xi^2 + 2(V(x_{i-\frac{1}{2}}^-) - V(x_{i-\frac{1}{2}}^+)) \geq 0, \\ -\xi & \text{otherwise.} \end{cases}$$

187 Up to now, we have defined the semi-discrete HPDG scheme (2.13) with fluxes discussed in (2.14)-(2.20).
 188 The integral of the numerical flux $\tilde{f}_{x,j+\frac{1}{2}}$ in the cell I_i in the scheme (2.13) is in general evaluated by directly
 189 applying standard Gauss quadrature rules in this cell. However, this approach may be inaccurate when dealing
 190 with the integral of the Hamiltonian-preserving numerical fluxes $\hat{f}_{i-\frac{1}{2},\xi}^\pm$ in the same way, since the range of ξ
 191 defined in (2.17) and (2.20) with $\xi \in J_j$ may span over more than one cell. Therefore, we have to be more
 192 careful when approximating the integrals involving fluxes $\hat{f}_{i-\frac{1}{2},\xi}^\pm$.

193 We now use the case of $\xi > 0$ to explain in details the approximation of these integrals. Here we assume
 194 $V(x)$ has a discontinuity at the cell interface $x_{i-\frac{1}{2}}$ with the jump $D = V_{i-\frac{1}{2}}^- - V_{i-\frac{1}{2}}^+ > 0$. The other cases,
 195 namely $D < 0$ or $\xi < 0$ can be treated in a similar fashion. To simplify the presentation, we assume that
 196 the mesh in ξ -direction is partitioned such that $0, \pm\sqrt{2D}$ are located at the cell interface. For the integral
 197 $\langle \xi \hat{f}_{i+\frac{1}{2},\xi}^-, \phi(x_{i+\frac{1}{2}}^-, \xi) \rangle_{J_j}$, it equals to $\langle \xi f(x_{i+\frac{1}{2}}^-, \xi), \phi(x_{i+\frac{1}{2}}^-, \xi) \rangle_{J_j}$ following the definition (2.14) and thus can be
 198 approximated by the standard Gauss quadrature rules in the cell J_j . The integral $\langle \xi \hat{f}_{i-\frac{1}{2},\xi}^+, \phi(x_{i-\frac{1}{2}}^+, \xi) \rangle_{J_j}$ is
 199 more complicated and the detailed approximation is given in the following with two cases considered.

200 If $D = V_{i-\frac{1}{2}}^- - V_{i-\frac{1}{2}}^+ > 0$ and $\xi_{j-\frac{1}{2}} \geq \sqrt{2D}$, with the definition (2.15) and (2.17), we have

$$201 \quad \langle \xi \hat{f}_{i-\frac{1}{2},\xi}^+, \phi(x_{i-\frac{1}{2}}^+, \xi) \rangle_{J_j} = \int_{\xi_{j-\frac{1}{2}}}^{\xi_{j+\frac{1}{2}}} \xi f(x_{i-\frac{1}{2}}^-, \tilde{\xi}) \phi(x_{i-\frac{1}{2}}^+, \xi) d\xi$$

$$202 \quad (2.21) \quad = \int_{\eta_{j-\frac{1}{2}}}^{\eta_{j+\frac{1}{2}}} \eta f(x_{i-\frac{1}{2}}^-, \eta) \phi(x_{i-\frac{1}{2}}^+, \sqrt{\eta^2 + 2D}) d\eta,$$

204 where $\eta = \sqrt{\xi^2 - 2D}$ and $\eta_{j\pm\frac{1}{2}} = \sqrt{\xi_{j\pm\frac{1}{2}}^2 - 2D}$. There are two possibilities for the locations of two end points
 205 $\eta_{j\pm\frac{1}{2}}$, though they may not be at the cell interface any more. They either fall into the same computational
 206 cell, or belong to different cells. In the former case, the integral (2.21) can be approximated by standard Gauss
 207 quadrature rules with sufficient accuracy. In the latter case, the integral can be approximated by a composite
 208 quadrature rule, where we first decompose the integration domain into the union of computational cells (or part
 209 of the computational cell near the end point) and then apply standard Gauss quadrature rules with sufficient
 210 accuracy.

211 If $D = V_{i-\frac{1}{2}}^- - V_{i-\frac{1}{2}}^+ > 0$ and $\xi_{j-\frac{1}{2}} < \sqrt{2D}$, it leads to that $\xi_{j+\frac{1}{2}} \leq \sqrt{2D}$ due to the assumption that $\sqrt{2D}$
 212 is located at the cell interface. With the definition (2.15) and (2.17), we have

$$213 \quad \langle \xi \hat{f}_{i-\frac{1}{2},\xi}^+, \phi(x_{i-\frac{1}{2}}^+, \xi) \rangle_{J_j} = \int_{\xi_{j-\frac{1}{2}}}^{\xi_{j+\frac{1}{2}}} \xi f(x_{i-\frac{1}{2}}^-, \tilde{\xi}) \phi(x_{i-\frac{1}{2}}^+, \xi) d\xi = \int_{\xi_{j-\frac{1}{2}}}^{\xi_{j+\frac{1}{2}}} \xi f(x_{i-\frac{1}{2}}^-, -\xi) \phi(x_{i-\frac{1}{2}}^+, \xi) d\xi,$$

215 which can be approximated by standard Gauss quadrature rules with sufficient accuracy.

216 **2.3. Positivity-preserving limiter .** In this section, we apply a positivity-preserving limiter to the
 217 HPDG scheme to provide an extra stabilizing mechanism, since the exact solution of the Liouville equation is
 218 always non-negative if the initial condition satisfies this.

219 Starting from the numerical solution f^n at time level n (for the initial condition, f^0 is simply taken as the
 220 standard L^2 projection of the analytical initial condition into \mathbb{V}_h^k), a positivity-preserving limiter can be applied
 221 to “limit” f^n to obtain a new function $f^{n,new}$, which preserves certain positive properties. The “limited” $f^{n,new}$
 222 is then advanced to the next time level with the SSP-RK time discretization methods (2.8). We present the
 223 limiting procedure to compute $f^{n,new}$ from f^n in the following and omit the superscript n for simplicity.

224 Denote $f_{ij}(x, \xi)$ as the DG approximation polynomial on the cell $K_{i,j}$ and \bar{f}_{ij} as the cell average of $f_{ij}(x, \xi)$
 225 on the cell K_{ij} . The ‘‘limited’’ function f^{new} is defined by

$$226 \quad (2.22) \quad f_{ij}^{new}(x, \xi) = \theta_1(f_{ij}(x, \xi) - \bar{f}_{ij}) + \bar{f}_{ij},$$

228 where $\theta_1 \in [0, 1]$ is determined by

$$229 \quad (2.23) \quad \theta_1 = \min \left\{ \frac{\bar{f}_{ij}}{f_{ij} - f_{\min}}, 1 \right\}, f_{\min} = \min_{(x, \xi) \in K_{ij}} f_{ij}(x, \xi).$$

231 Clearly the cell average of $f_{ij}^{new}(x, \xi)$ over K_{ij} is still \bar{f}_{ij} and $f_{ij}^{new}(x, \xi) \geq 0$ in the cell K_{ij} if $\bar{f}_{ij} \geq 0$. We refer
 232 readers to [25, 24, 37, 36] and the references cited therein for more detailed discussions on the positive-preserving
 233 and maximum-principle-satisfying limiter.

234 *Remark 2.1.* In order to successfully apply the positivity-preserving limiter (2.22), one needs the assump-
 235 tion that $\bar{f}_{ij} \geq 0$. We will analytically prove that the cell average of the DG numerical solution at the next
 236 time level t^{n+1} satisfies this assumption in Theorem 3.3.

237 *Remark 2.2.* For numerical implementation, the exact value f_{\min} in (2.23) can be easily found for $k = 1, 2$
 238 by comparing a finite set of special points. However, the exact value of f_{\min} is difficult to compute for
 239 higher order polynomials ($k > 2$), especially for multi-dimensional cases. One practical approach is to use
 240 $\min_{(x, \xi) \in G} f_{ij}(x, \xi)$ as an approximation, where the set G contains the Gauss-Lobatto quadrature points inside
 241 each computational cell and all the quadrature points used to evaluate the integrals in (2.21). As a result
 242 of this, the ‘‘limited’’ function f^{new} is no longer positive everywhere, instead we have $f^{new}(x, \xi) \geq 0$ for any
 243 $(x, \xi) \in G$. Note that Theorem 3.3 still holds for such case, since the integrals in (3.11) are non-negative after
 244 applying a (composite) quadrature rule based on the points in G .

245 *Remark 2.3.* The positivity-preserving limiter (2.22) can be easily extended to be a bound-preserving
 246 limiter to enforce the ‘‘limited’’ function $f^{new} \in [0, 1]$ and ensure extra stability if the initial condition satisfies
 247 it, following the maximum-principle-satisfying limiter in [36]. If the potential $V(x)$ is smooth, it can be
 248 analytically proved that the numerical solutions of the DG methods coupling with the bound-preserving limiter
 249 stay within the range of $[0, 1]$, as did in [36]. When the potential $V(x)$ is discontinuous, the first order finite
 250 volume Hamiltonian-preserving method in [19] is shown to be L^∞ stable, and the L^∞ norm is shown to grow
 251 with an amplification factor of order $1 + O(\Delta t)$. Thus the bound-preserving property is not clear for the finite
 252 volume method which is equivalent with the DG methods of $k = 0$. Therefore we do not engage in depth the
 253 bound-preserving property for the high order HPDG methods. We numerically apply the bound-preserving
 254 limiter to test its performances in Examples 5.2 and 5.3.

255 **3. Positivity and L^1 stability.** In this section, we investigate the positivity-preserving property and L^1
 256 stability of the proposed DG scheme in Section 2, for solving the Liouville equation (2.1) with discontinuous
 257 potential. The study is based on the simple first order Euler forward temporal discretization. High-order
 258 SSP-RK time discretizations will keep the validity of the properties, since they can be written as convex
 259 combinations of forward Euler steps.

260 A fully discrete scheme for the semi-discrete scheme (2.13) with Euler forward is given by

$$261 \quad (3.1) \quad \left(\frac{f^{n+1} - f}{\Delta t}, \phi \right)_{K_{ij}} - (\xi f, \phi_x)_{K_{ij}} + \left\langle \xi \hat{f}_{i+\frac{1}{2}, \xi}^-, \phi(x_{i+\frac{1}{2}}^-, \xi) \right\rangle_{J_j} - \left\langle \xi \hat{f}_{i-\frac{1}{2}, \xi}^+, \phi(x_{i-\frac{1}{2}}^+, \xi) \right\rangle_{J_j}$$

$$262 \quad + (V_x f, \phi_\xi)_{K_{ij}} - \left\langle V_x \tilde{f}_{x, j+\frac{1}{2}}, \phi(x, \xi_{j+\frac{1}{2}}^-) \right\rangle_{I_i} + \left\langle V_x \tilde{f}_{x, j-\frac{1}{2}}, \phi(x, \xi_{j-\frac{1}{2}}^+) \right\rangle_{I_i} = 0,$$

263 where we omit the superscript of $f^{n, new}$ and still use f to denote the limited solution by the positivity-preserving
 264 limiter discussed in Section (2.3) at time level n . Here $\tilde{f}_{x, j+\frac{1}{2}}$ are the upwind fluxes defined in (2.6). $\hat{f}_{i+\frac{1}{2}, \xi}^\pm$
 265 are the the Hamiltonian-preserving fluxes defined in Section 2.2 at the discontinuity point $x_{i+\frac{1}{2}}$ of $V(x)$, while
 266 $\hat{f}_{i+\frac{1}{2}, \xi}^+ = \hat{f}_{i+\frac{1}{2}, \xi}^- = \hat{f}_{i+\frac{1}{2}, \xi}$ defined in (2.5) for the smooth point $x_{i+\frac{1}{2}}$ of $V(x)$.

267 The first order version of the proposed DG methods (with polynomial degree $k = 0$) reduces to the finite
 268 volume methods designed in [19], and the positivity-preserving limiter (2.22) is not active. Therefore, this first
 269 order method has the properties of being positive, L^1 -contracting and L^∞ stable as studied in [19]. Next, we
 270 would like to prove that some properties also hold for the high order DG methods with polynomials of arbitrary
 271 degree. We first show in the following lemma that one-dimensional integral at the cell boundary is bounded
 272 by the cell average.

273 **LEMMA 3.1.** *For any $\varphi(x, \xi) \in \mathbb{P}^k(K_{ij})$ and $\varphi(x, \xi) \geq 0$, there exists a positive constant $\omega = \omega(k)$ depending*
 274 *on the polynomial degree k , such that*

$$275 \quad (3.2) \quad \int_{J_j} \varphi(x_{i-\frac{1}{2}}^+, \xi) d\xi \leq \frac{\omega}{\Delta x} \overline{(\varphi)}_{K_{ij}}, \quad \int_{J_j} \varphi(x_{i+\frac{1}{2}}^-, \xi) d\xi \leq \frac{\omega}{\Delta x} \overline{(\varphi)}_{K_{ij}},$$

$$276 \quad (3.3) \quad \int_{I_i} \varphi(x, \xi_{j-\frac{1}{2}}^+) dx \leq \frac{\omega}{\Delta \xi} \overline{(\varphi)}_{K_{ij}}, \quad \int_{I_i} \varphi(x, \xi_{j-\frac{1}{2}}^+) dx \leq \frac{\omega}{\Delta \xi} \overline{(\varphi)}_{K_{ij}},$$

277
 278 where $\overline{(\varphi)}_{K_{ij}}$ denotes the integral of $\varphi(x, \xi)$ on the cell K_{ij} .

279 *Proof.* Denote $\{\zeta_\ell\}_{\ell=0}^k$ as the Legendre-Gauss-Lobatto quadrature points in $[-1, 1]$ and $\{\omega_\ell\}_{\ell=0}^k$ as the
 280 associated quadrature weights. By the Legendre-Gauss-Lobatto quadrature rule with $k + 1$ points which is
 281 exact for polynomials of degree up to $2k - 1$, we have

$$282 \quad (3.4) \quad \begin{aligned} \overline{(\varphi)}_{K_{ij}} &= \int_{J_j} \int_{I_i} \varphi(x, \xi) dx d\xi = \sum_{\ell=0}^k \omega_\ell \Delta x \int_{J_j} \varphi(x_i + \frac{\Delta x}{2} \zeta_\ell, \xi) d\xi \\ &\geq \omega_0 \Delta x \int_{J_j} \varphi(x_{i-\frac{1}{2}}, \xi) d\xi + \omega_k \Delta x \int_{J_j} \varphi(x_{i+\frac{1}{2}}, \xi) d\xi, \end{aligned}$$

283
 284 where the last inequality is based on the fact that $\varphi(x, \xi) \geq 0$ and $\omega_\ell > 0$ for $\ell = 0, \dots, k$. Since $\omega_0 = \omega_k$, we
 285 obtain (3.2) by setting $\omega = 1/\omega_0$. (3.3) can be proved similarly. \square

286 *Remark 3.2.* The proof is valid for $k > 0$. In particular, $\omega = 2$ when $k = 1$ and $\omega = 6$ when $k = 2$,
 287 according to the quadrature weights. For the case when $k = 0$, (3.2) and (3.3) hold with $\omega = 1$, since $\varphi(x, \xi)$
 288 is a constant function with $k = 0$.

289 Next we investigate the positivity of the fully discrete scheme (3.1). We show in the following theorem
 290 that by adding a positivity-preserving limiter discussed in Section 2.3 to the HPDG methods, and coupling
 291 with the time evolution by Euler forward method, the resulting Hamiltonian-preserving scheme (3.1) preserves
 292 the positivity in the sense that the cell averages are always positive if they are positive initially, under
 293 suitable CFL conditions. We remark here that the proof can not be trivially extended from the classical DG
 294 methods for hyperbolic conservation laws in [36, 24], due to the complication appeared when the potential
 295 $V(x)$ is discontinuous.

296 **THEOREM 3.3 (Positivity).** *The solution f^{n+1} of (3.1) satisfies $\overline{(f^{n+1})}_{K_{ij}} \geq 0$ under the CFL condition*

$$297 \quad (3.5) \quad \omega \Delta t \left(\frac{\max |\xi|}{\Delta x} + \frac{\max_i \sup_{x \in \text{int}(I_i)} |V_x|}{\Delta \xi} \right) \leq 1,$$

298
 299 where ω is the positive constant presented in Lemma 3.1 and $\text{int}(I_m)$ denotes the interior of the cell I_m .

300 *Proof.* For simplicity, we consider the case when $\xi > 0$ and 0 is located at the cell interface in ξ -direction,
 301 $V(x)$ has only one discontinuity point located at the cell interface $x_{m-\frac{1}{2}}$ with jump $D = V_{m-\frac{1}{2}}^- - V_{m-\frac{1}{2}}^+ > 0$,
 302 and $V'(x) < 0$ at smooth points. The other cases, namely, when $\xi < 0$ or the potential $V(x)$ has several
 303 discontinuity points with positive or negative jumps, or $V'(x) > 0$, can be discussed in the similar fashion. We
 304 further assume that the mesh is partitioned such that $0, \pm\sqrt{2D}$ are grid points in ξ -direction.

305 The fully discrete scheme (3.1) with the test function taken as $\phi \equiv 1$ yields

$$306 \quad (3.6) \quad \frac{\overline{(f^{n+1})}_{K_{ij}} - \overline{(f)}_{K_{ij}}}{\Delta t} + \left\langle \xi \hat{f}_{i+\frac{1}{2}, \xi}^- \right\rangle_{J_j} - \left\langle \xi \hat{f}_{i-\frac{1}{2}, \xi}^+ \right\rangle_{J_j} - \left\langle V_x \tilde{f}_{x, j+\frac{1}{2}} \right\rangle_{I_i} + \left\langle V_x \tilde{f}_{x, j-\frac{1}{2}} \right\rangle_{I_i} = 0.$$

308 Here f is the limited solution at time level n after applying the positivity-preserving limiter, and thus $f(x, \xi) \geq$
 309 0 , $(x, \xi) \in K_{ij}$ for $i = 1, \dots, N_x$, $j = 1, \dots, N_\xi$.

310 Recall that the discontinuity of $V(x)$ is located at $x_{m-\frac{1}{2}}$ and $\sqrt{2D}$ is a grid point in the ξ -direction. When
 311 $i = m$, with the Hamiltonian-preserving fluxes defined in Section 2.2, we have

312 • if $\xi_{j-\frac{1}{2}}^2 - 2D \geq 0$,

$$313 \quad (3.7) \quad \frac{\overline{(f^{n+1})}_{K_{mj}} - \overline{(f)}_{K_{mj}}}{\Delta t} + \int_{J_j} \xi f(x_{m+\frac{1}{2}}^-, \xi) d\xi - \int_{\eta_{j-\frac{1}{2}}}^{\eta_{j+\frac{1}{2}}} \eta f(x_{m-\frac{1}{2}}^-, \eta) d\eta$$

$$314 \quad - \left\langle V_x \tilde{f}_{x, j+\frac{1}{2}} \right\rangle_{I_m} + \left\langle V_x \tilde{f}_{x, j-\frac{1}{2}} \right\rangle_{I_m} = 0,$$

315 where $\eta = \sqrt{\xi^2 - 2D}$ and $\eta_{j\pm\frac{1}{2}} = \sqrt{\xi_{j\pm\frac{1}{2}}^2 - 2D}$;

316 • if $\xi_{j-\frac{1}{2}}^2 - 2D < 0$,

$$317 \quad (3.8) \quad \frac{\overline{(f^{n+1})}_{K_{mj}} - \overline{(f)}_{K_{mj}}}{\Delta t} + \int_{J_j} \xi f(x_{m+\frac{1}{2}}^-, \xi) d\xi - \int_{J_j} \xi f(x_{m-\frac{1}{2}}^+, -\xi) d\xi$$

$$318 \quad - \left\langle V_x \tilde{f}_{x, j+\frac{1}{2}} \right\rangle_{I_m} + \left\langle V_x \tilde{f}_{x, j-\frac{1}{2}} \right\rangle_{I_m} = 0.$$

319 By Lemma 3.1 and (2.6), we have

$$320 \quad (3.9) \quad \int_{J_j} \xi f(x_{m+\frac{1}{2}}^-, \xi) d\xi \leq |\xi_{j+\frac{1}{2}}| \int_{J_j} f(x_{m+\frac{1}{2}}^-, \xi) d\xi \leq \frac{\omega |\xi_{j+\frac{1}{2}}|}{\Delta x} (\overline{(f)}_{K_{mj}}),$$

$$321 \quad (3.10) \quad - \left\langle V_x \tilde{f}_{x, j+\frac{1}{2}} \right\rangle_{I_m} = - \int_{I_m} V_x f(x, \xi_{j+\frac{1}{2}}^-) dx \leq \frac{\omega \sup_{x \in \text{int}(I_m)} |V_x|}{\Delta \xi} \overline{(f)}_{K_{mj}},$$

323 where $\text{int}(I_m)$ denotes the interior of the cell I_m , i.e. $\text{int}(I_m) = (x_{m-\frac{1}{2}}, x_{m+\frac{1}{2}})$. Since $V(x)$ is Lipschitz
 324 continuous for $x \in \text{int}(I_m)$ under our assumption, $\sup_{x \in \text{int}(I_m)} |V_x|$ has a finite upper bound. Notice that
 325 $\eta \geq 0, \eta_{j\pm\frac{1}{2}} \geq 0$, combining with the assumption that $\xi > 0$, $V'(x) < 0$ at smooth points and f being
 326 non-negative, yielding

$$327 \quad (3.11) \quad \int_{\eta_{j-\frac{1}{2}}}^{\eta_{j+\frac{1}{2}}} \eta f(x_{m-\frac{1}{2}}^-, \eta) d\eta \geq 0, \quad \int_{J_j} \xi f(x_{m-\frac{1}{2}}^+, -\xi) d\xi \geq 0,$$

328 and

$$330 \quad (3.12) \quad \left\langle V_x \tilde{f}_{x, j-\frac{1}{2}} \right\rangle_{I_i} = \left\langle V_x f(x, \xi_{j-\frac{1}{2}}^-) \right\rangle_{I_i} \leq 0.$$

332 Therefore, we have, by (3.7)-(3.12),

$$333 \quad (3.13) \quad \overline{(f)}_{K_{mj}}^{n+1} \geq \left(1 - \omega \Delta t \left(\frac{|\xi_{j+\frac{1}{2}}|}{\Delta x} + \frac{\sup_{x \in \text{int}(I_m)} |V_x|}{\Delta \xi} \right) \right) \overline{(f)}_{K_{mj}}.$$

335 This proves that $\overline{(f)}_{K_{mj}}^{n+1} \geq 0$ under the CFL condition (3.5).

336 For the case when $i \neq m$, the fully scheme (3.1) is simply the standard DG scheme with upwind fluxes.
 337 Similar proof can be found in [37, 36], and thus is omitted. \square

338 *Remark 3.4.* The CFL condition (3.5) in Theorem 3.3 is similar to the CFL condition (2.9). However, $|V_x|$
 339 now represents the derivative of the potential $V(x)$ at its Lipschitz continuous region and thus has an $O(1)$
 340 upper bound, since $V(x)$ is only discontinuous at grid points under our assumption. Thus our proposed scheme
 341 has a hyperbolic CFL condition.

342 Now we study the stability property of the proposed scheme.

343 **THEOREM 3.5 (L^1 contracting).** *Assume that $f(x, \xi) = 0$ at the boundary and no particles come from*
 344 *outside of the domain $[-L, L] \times [-A_c, A_c]$. Then the solution f^{n+1} of (3.1) is L^1 -contracting, i.e.*

$$345 \quad (3.14) \quad \sum_{ij} |(\overline{f})^{n+1}|_{K_{ij}} \leq \sum_{ij} |(\overline{f})|_{K_{ij}}$$

346
 347 under the CFL condition (3.5).

348 *Remark 3.6.* Due to the linearity of the scheme (3.1), the equation for the error between the analytical
 349 solution and the numerical solution is the same as the scheme (3.1) itself. Thus we assume there is no error at
 350 the boundary, and zero Dirichlet boundary conditions can be considered as a simplified case.

Remark 3.7. After applying the positivity-preserving limiter (2.22), the limited numerical solution at time
 lever $n + 1$, i.e. $f^{n+1, new}$ is non-negative and also maintains the cell average of the solution f^{n+1} . Thus we
 have $(|f|)^{n+1, new}_{K_{ij}} = |(\overline{f})^{n+1, new}|_{K_{ij}} = |(\overline{f})^{n+1}|_{K_{ij}}$. Combining with (3.14) leads to

$$\|f^{n+1, new}\|_{L^1} \leq \|f^{n, new}\|_{L^1},$$

351 i.e., the L^1 stability property of the numerical solutions.

352 *Proof.* For simplicity, we again consider the case when $V(x)$ has only one discontinuity at the cell interface
 353 $x_{m-\frac{1}{2}}$ with jump $D = V_{m-\frac{1}{2}}^- - V_{m-\frac{1}{2}}^+ > 0$, and $V'(x) < 0$ at smooth points. The other cases can be discussed
 354 similarly. We again assume that the mesh is partitioned such that $0, \pm\sqrt{2D}$ are grid points in ξ -direction. We
 355 further assume that $\xi_{N_{\xi+\frac{1}{2}}} > \sqrt{2D}$ to include all the possible behaviors of the particles such as crossing the
 356 potential barrier with increased/reduced momentum, or being reflected.

357 By taking the test function $\phi \equiv 1$ in the fully discrete scheme (3.1), we can rewrite it as

$$358 \quad (3.15) \quad \frac{(\overline{f}^{n+1})_{K_{ij}} - (\overline{f})_{K_{ij}}}{\Delta t} = \underbrace{-\left\langle \xi \hat{f}_{i+\frac{1}{2}, \xi}^- \right\rangle_{J_j} + \left\langle \xi \hat{f}_{i-\frac{1}{2}, \xi}^+ \right\rangle_{J_j} + \left\langle V_x \tilde{f}_{x, j+\frac{1}{2}} \right\rangle_{I_i} - \left\langle V_x \tilde{f}_{x, j-\frac{1}{2}} \right\rangle_{I_i}}_{R_{ij}}.$$

359

Here f is the limited solution at time level n after applying the positivity-preserving limiter, and thus $f(x, \xi) \geq$
 $0, (x, \xi) \in K_{ij}$ for $i = 1, \dots, N_x, j = 1, \dots, N_{\xi}$. By Theorem (3.3), we have $(\overline{f}^{n+1})_{K_{ij}} \geq 0$ under the CFL
 condition (3.5). Therefore, to show the L^1 contracting property (3.14), we only need to prove that

$$\sum_{ij} R_{ij} \leq 0.$$

360 With the upwind fluxes defined in (2.5) and (2.6), and the Hamiltonian-preserving numerical fluxes defined
 361 in (2.14), (2.15), (2.18) and (2.19), we have

362 (1) if $\xi_j > 0, i \neq m$,

$$363 \quad (3.16) \quad R_{ij} = - \int_{J_j} \xi f(x_{i+\frac{1}{2}}^-, \xi) d\xi + \int_{J_j} \xi f(x_{i-\frac{1}{2}}^-, \xi) d\xi + \left\langle V_x \tilde{f}_{x, j+\frac{1}{2}} \right\rangle_{I_i} - \left\langle V_x \tilde{f}_{x, j-\frac{1}{2}} \right\rangle_{I_i};$$

365 (2) if $\xi_j < 0, i \neq m - 1$,

$$366 \quad (3.17) \quad R_{ij} = - \int_{J_j} \xi f(x_{i+\frac{1}{2}}^+, \xi) d\xi + \int_{J_j} \xi f(x_{i-\frac{1}{2}}^+, \xi) d\xi + \left\langle V_x \tilde{f}_{x, j+\frac{1}{2}} \right\rangle_{I_i} - \left\langle V_x \tilde{f}_{x, j-\frac{1}{2}} \right\rangle_{I_i};$$

368 (3) if $\xi_j > 0, i = m$,

$$369 \quad (3.18) \quad R_{ij} = - \int_{J_j} \xi f(x_{i+\frac{1}{2}}^-, \xi) d\xi + \left\langle \xi \hat{f}_{i-\frac{1}{2}, \xi}^+ \right\rangle_{J_j} + \left\langle V_x \tilde{f}_{x, j+\frac{1}{2}} \right\rangle_{I_i} - \left\langle V_x \tilde{f}_{x, j-\frac{1}{2}} \right\rangle_{I_i};$$

370

371 (4) if $\xi_j < 0$, $i = m - 1$,

372 (3.19)
$$R_{ij} = -\left\langle \xi \hat{f}_{i+\frac{1}{2}, \xi}^- \right\rangle_{J_j} + \int_{J_j} \xi f(x_{i-\frac{1}{2}}^+, \xi) d\xi - \left\langle V_x \tilde{f}_{x, j+\frac{1}{2}} \right\rangle_{I_i} + \left\langle V_x \tilde{f}_{x, j-\frac{1}{2}} \right\rangle_{I_i}.$$

373

374 Summing up (3.16)-(3.19) over all the elements i, j , we have

375 (3.20)
$$\begin{aligned} \sum_{ij} R_{ij} &= \sum_{\xi_j > 0} \left(\left\langle \xi \hat{f}_{m-\frac{1}{2}, \xi}^+ \right\rangle_{J_j} - \int_{J_j} \xi f(x_{m-\frac{1}{2}}^-, \xi) d\xi \right) \\ &\quad - \sum_{\xi_j < 0} \left(\left\langle \xi \hat{f}_{m-\frac{1}{2}, \xi}^- \right\rangle_{J_j} - \int_{J_j} \xi f(x_{m-\frac{1}{2}}^+, \xi) d\xi \right), \end{aligned}$$

376

due to zero boundary condition, and all the numerical fluxes in the ξ direction cancel after the summation. To simplify the presentation, we omit the subscript $m - \frac{1}{2}$ in the following. Let us introduce the notations

$$\eta = \sqrt{\xi^2 - 2D}, \quad \eta_{j\pm\frac{1}{2}} = \sqrt{\xi_{j\pm\frac{1}{2}}^2 - 2D}, \quad \eta' = -\sqrt{\xi^2 + 2D}, \quad \eta'_{j\pm\frac{1}{2}} = -\sqrt{\xi_{j\pm\frac{1}{2}}^2 + 2D}.$$

377 By a change of variables as in (2.21) and utilizing the definition of the Hamiltonian-preserving numerical fluxes
378 \hat{f}^\pm in Section 2.2, we obtain

379 (3.21)
$$\begin{aligned} \sum_{ij} R_{ij} &= \sum_{\xi_{j-\frac{1}{2}} \geq \sqrt{2D}} \int_{\eta_{j-\frac{1}{2}}}^{\eta_{j+\frac{1}{2}}} \eta f(x^-, \eta) d\eta + \sum_{0 \leq \xi_{j-\frac{1}{2}} < \sqrt{2D}} \int_{J_j} \xi f(x^-, -\xi) d\xi \\ &\quad - \sum_{\xi_j > 0} \int_{J_j} \xi f(x^-, \xi) d\xi + \sum_{\xi_j < 0} \int_{J_j} \xi f(x^+, \xi) d\xi - \sum_{\xi_{j+\frac{1}{2}} \leq 0} \int_{\eta'_{j-\frac{1}{2}}}^{\eta'_{j+\frac{1}{2}}} \eta' f(x^+, \eta') d\eta' \\ &= \int_0^{\sqrt{\xi_{N_\xi+\frac{1}{2}}^2 - 2D}} \eta f(x^-, \eta) d\eta - \int_{-\sqrt{2D}}^0 \xi f(x^+, \xi) d\xi \\ &\quad - \int_0^{\xi_{N_\xi+\frac{1}{2}}} \xi f(x^-, \xi) d\xi + \int_{-\xi_{N_\xi+\frac{1}{2}}}^0 \xi f(x^+, \xi) d\xi - \int_{-\sqrt{\xi_{N_\xi+\frac{1}{2}}^2 + 2D}}^{-\sqrt{2D}} \eta' f(x^+, \eta') d\eta' \\ &= - \int_{\sqrt{\xi_{N_\xi+\frac{1}{2}}^2 - 2D}}^{\xi_{N_\xi+\frac{1}{2}}} \xi f(x^-, \xi) d\xi + \int_{-\sqrt{\xi_{N_\xi+\frac{1}{2}}^2 + 2D}}^{-\xi_{N_\xi+\frac{1}{2}}} \xi f(x^+, \xi) d\xi \leq 0, \end{aligned}$$

380

381 where the second equality is due to the fact that 0 and $\pm\sqrt{2D}$ locate at the cell interfaces in the ξ -direction,
382 and the last inequality follows from the fact that f is non-negative and no particles come from outside of the
383 domain according to our assumption. \square

384 **4. Extension to higher dimensions.** In this section, we extend our proposed scheme for the Liouville
385 equation under 1D1V setting to higher dimensions. As an example, we consider the following two-dimensional
386 Liouville equation

387 (4.1)
$$f_t + \xi f_x + \eta f_y - V_x f_\xi - V_y f_\eta = 0,$$

388

in the 2D2V setting. Let \mathcal{T}_h be uniform partition of the computational domain with the meshes $K_{ij\kappa\ell} = I_i^{(x)} \times I_j^{(y)} \times J_\kappa^{(\xi)} \times J_\ell^{(\eta)} = [x_{i-\frac{1}{2}}, x_{i+\frac{1}{2}}] \times [y_{j-\frac{1}{2}}, y_{j+\frac{1}{2}}] \times [\xi_{\kappa-\frac{1}{2}}, \xi_{\kappa+\frac{1}{2}}] \times [\eta_{\ell-\frac{1}{2}}, \eta_{\ell+\frac{1}{2}}]$ and the cell interfaces located at $x_{i+\frac{1}{2}}, y_{j+\frac{1}{2}}, \xi_{\kappa+\frac{1}{2}}, \eta_{\ell+\frac{1}{2}}$ in each direction. The mesh size is denoted by $\Delta x = x_{i+\frac{1}{2}} - x_{i-\frac{1}{2}}$, $\Delta y = y_{j+\frac{1}{2}} - y_{j-\frac{1}{2}}$, $\Delta \xi = \xi_{\kappa+\frac{1}{2}} - \xi_{\kappa-\frac{1}{2}}$, $\Delta \eta = \eta_{\ell+\frac{1}{2}} - \eta_{\ell-\frac{1}{2}}$. Let us define a high dimensional DG finite element approximation space

$$\mathbb{W}_h^k = \{v : v|_{K_{ij\kappa\ell}} \in P^k(K_{ij\kappa\ell}), K_{ij\kappa\ell} \in \mathcal{T}_h\}.$$

389 Similarly to the one-dimensional case, the semi-discrete HPDG scheme for the 2D2V Liouville equation
 390 (4.1) is defined as: for any test function $\phi \in \mathbb{W}_h^k$, we have

$$\begin{aligned}
 & (f_t, \phi)_{K_{ij\kappa\ell}} - (\xi f, \phi_x)_{K_{ij\kappa\ell}} - (\eta f, \phi_y)_{K_{ij\kappa\ell}} + (V_x f, \phi_\xi)_{K_{ij\kappa\ell}} + (V_y f, \phi_\eta)_{K_{ij\kappa\ell}} \\
 & + \left\langle \xi \hat{f}_{i+\frac{1}{2}, j, \xi, \eta}^-, \phi(x_{i+\frac{1}{2}}^-, y, \xi, \eta) \right\rangle_{I_j^{(y)} \times J_\kappa^{(\xi)} \times J_\ell^{(\eta)}} - \left\langle \xi \hat{f}_{i-\frac{1}{2}, j, \xi, \eta}^+, \phi(x_{i-\frac{1}{2}}^+, y, \xi, \eta) \right\rangle_{I_j^{(y)} \times J_\kappa^{(\xi)} \times J_\ell^{(\eta)}} \\
 & + \left\langle \eta \hat{f}_{i, j+\frac{1}{2}, \xi, \eta}^-, \phi(x, y_{j+\frac{1}{2}}^-, \xi, \eta) \right\rangle_{I_i^{(x)} \times J_\kappa^{(\xi)} \times J_\ell^{(\eta)}} - \left\langle \eta \hat{f}_{i, j-\frac{1}{2}, \xi, \eta}^+, \phi(x, y_{j-\frac{1}{2}}^+, \xi, \eta) \right\rangle_{I_i^{(x)} \times J_\kappa^{(\xi)} \times J_\ell^{(\eta)}} \\
 & - \left\langle V_x \tilde{\tilde{f}}_{x, y, \kappa+\frac{1}{2}, \eta}, \phi(x, y, \xi_{\kappa+\frac{1}{2}}^-, \eta) \right\rangle_{I_i^{(x)} \times I_j^{(y)} \times J_\ell^{(\eta)}} + \left\langle V_x \tilde{\tilde{f}}_{x, y, \kappa-\frac{1}{2}, \eta}, \phi(x, y, \xi_{\kappa-\frac{1}{2}}^+, \eta) \right\rangle_{I_i^{(x)} \times I_j^{(y)} \times J_\ell^{(\eta)}} \\
 & - \left\langle V_y \tilde{\tilde{f}}_{x, y, \xi, \ell+\frac{1}{2}}, \phi(x, y, \xi, \eta_{\ell+\frac{1}{2}}^-) \right\rangle_{I_i^{(x)} \times I_j^{(y)} \times J_\ell^{(\xi)}} + \left\langle V_y \tilde{\tilde{f}}_{x, y, \xi, \ell-\frac{1}{2}}, \phi(x, y, \xi, \eta_{\ell-\frac{1}{2}}^+) \right\rangle_{I_i^{(x)} \times I_j^{(y)} \times J_\ell^{(\xi)}} \\
 & = 0,
 \end{aligned}$$

393 where numerical fluxes $\tilde{\tilde{f}}$ and \hat{f} in the ξ - and η -direction take the upwind fluxes as defined in (2.6). We
 394 also define the fluxes \hat{f}^\pm and $\tilde{\tilde{f}}^\pm$ at the cell interface to account for the potential discontinuous potential.
 395 They are defined following the same procedure as in Section 2.2 to preserve a constant Hamiltonian across the
 396 potential barrier. The two-dimensional version of the positivity-preserving limiter, similar to those in (2.22),
 397 can be applied to enhance the stability and preserve non-negativity of density distribution f . The third order
 398 SSP-RK temporal discretization (2.8) can again be utilized to advance in time.

399 **5. Numerical results.** In this section, we present some numerical tests to demonstrate the performance
 400 of the proposed HPDG scheme with the positivity-preserving limiter. In the examples, the time step size is
 401 set as $\Delta t = \text{CFL} \cdot \Delta x$, where CFL is taken as indicated in (3.5). For the accuracy tests (e.g., Example 5.1),
 402 we adjust the time step Δt as $\Delta t = \text{CFL} \cdot \Delta x^{4/3}$ for P^3 case so that the temporal and spatial error are of the
 403 same level.

404 *Example 5.1. Accuracy test*

405 In this example, we consider the following Liouville equation in a 1D1V setting

$$406 \quad (5.1) \quad f_t + \xi f_x - V_x f_\xi = (x + \xi - 1) \cos(x + \xi - t), \quad (x, \xi) \in [-\pi, \pi] \times [-\pi, \pi]$$

with the continuous potential $V(x) = -\frac{x^2}{2}$ to test the accuracy of the HPDG scheme. The initial condition is
 set to be

$$f(x, \xi, 0) = \sin(x + \xi),$$

and periodic boundary conditions are applied. The exact solution takes the form

$$f(x, \xi, t) = \sin(x + \xi - t).$$

408 We perform numerical simulations up to $t = 0.1$ and list the L^1 and L^∞ errors and orders of accuracy
 409 for the HPDG method with polynomials of degree k ($k = 1, 2, 3$) in Table 5.1. We can see that for all three
 410 polynomial spaces, the proposed DG scheme achieved the optimal $k + 1$ -th order of accuracy.

411 *Example 5.2. 1D1V problem with an exact L^∞ solution*

412 In this example, we consider one-dimensional Liouville equation (2.1) with a discontinuous potential $V(x)$ given
 413 by

$$414 \quad (5.2) \quad V(x) = \begin{cases} 0.2, & x < 0, \\ 0, & x > 0, \end{cases}$$

415 and the initial condition set as

$$416 \quad (5.3) \quad f(x, \xi, 0) = \begin{cases} 1, & x \leq 0, \xi > 0, \sqrt{x^2 + \xi^2} < 1, \\ 1, & x \geq 0, \xi < 0, \sqrt{x^2 + \xi^2} < 1, \\ 0, & \text{otherwise.} \end{cases}$$

417

TABLE 5.1

Errors and orders of accuracy for the HPDG method solving the Liouville equation with a continuous potential in Example 5.1.

$N_x \times N_\xi$	P^1				P^2			
	L^1 error	Order	L^∞ error	Order	L^1 error	Order	L^∞ error	Order
30×30	1.58E-02		1.93E-03		2.71E-04		7.46E-05	
40×40	8.89E-03	2.00	1.08E-03	2.01	1.14E-04	3.00	3.12E-05	3.04
50×50	5.69E-03	2.00	6.88E-04	2.03	5.74E-05	3.09	1.59E-05	3.00
75×75	2.52E-03	2.01	3.04E-04	2.02	1.68E-05	3.03	4.99E-06	2.86
100×100	1.41E-03	2.01	1.71E-04	1.99	7.05E-06	3.02	2.12E-06	2.98

$N_x \times N_\xi$	P^3		L^∞ error	Order
	L^1 error	Order		
30×30	4.82E-06		1.68E-06	
40×40	1.57E-06	3.91	5.07E-07	4.16
50×50	6.19E-07	4.16	2.09E-07	3.97
75×75	1.21E-07	4.02	4.07E-08	4.04
100×100	3.83E-08	4.01	1.27E-08	4.04

418 The computational domain is set as $[-1.5, 1.5] \times [-1.5, 1.5]$. This is a 1D1V problem with an exact L^∞ solution
 419 available, and the exact solution at time $t = 1$, as constructed in [19], is given by

$$420 \quad (5.4) \quad f(x, \xi, 1) = \begin{cases} 1, & x \geq 0, \xi < \sqrt{0.4}, \xi \geq x, \\ 1, & 0 \leq x < 1, \xi < 0, \xi > \frac{x - \sqrt{2 - x^2}}{2}, \\ 1, & x \leq 0, x < (1 - \frac{0.6 - \xi^2}{0.4 + \xi^2})\xi, -\sqrt{0.6} < \xi < x, \\ 1, & -1 < x \leq 0, \xi > 0, \xi < \frac{x + \sqrt{2 - x^2}}{2}, \\ 1, & x \geq 0, x > (1 - \frac{\sqrt{1.4 - \xi^2}}{\sqrt{\xi^2 - 0.4}})\xi, \xi > x, \sqrt{0.4} < \xi < \sqrt{1.4}, \\ 0, & \text{otherwise.} \end{cases}$$

421 We perform numerical simulations on 100×100 meshes for the proposed DG method with P^2 polynomials
 422 up to $t = 1$. Figure 5.1 shows the initial solution (taken as the standard L^2 projection of the initial condition
 423 (5.3)), the “limited” initial solution after applying the total variation bounded (TVB) minmod limiter [10]
 424 or the bound-preserving limiter to keep $0 \leq f(x, \xi, 0) \leq 1$. Figure 5.2 shows the numerical solution at $t = 1$
 425 obtained by the HPDG method only, numerical solution obtained by the HPDG method with the TVB minmod
 426 limiter, and numerical solution obtained by the HPDG method with the bound-preserving limiter. We observe
 427 that there are some oscillations in the plots of the initial condition when projecting the solutions to the piece-
 428 wise P^2 polynomial space, since the initial solution is discontinuous. When either limiter is applied, there
 429 are no oscillations in the numerical solutions. For this example, the boundary-preserving limiter can achieve
 430 good non-oscillatory results as the TVB minmod limiter, and a sharp and smooth interface can be observed
 431 numerically.

432 Example 5.3. 1D1V problem with a measure-valued solution

433 In this example, we consider one-dimensional Liouville equation (2.1) with the same potential (5.2) as in
 434 Example 5.1. The initial condition is given by

$$435 \quad (5.5) \quad f(x, \xi, 0) = \delta(\xi - \nu(x)),$$

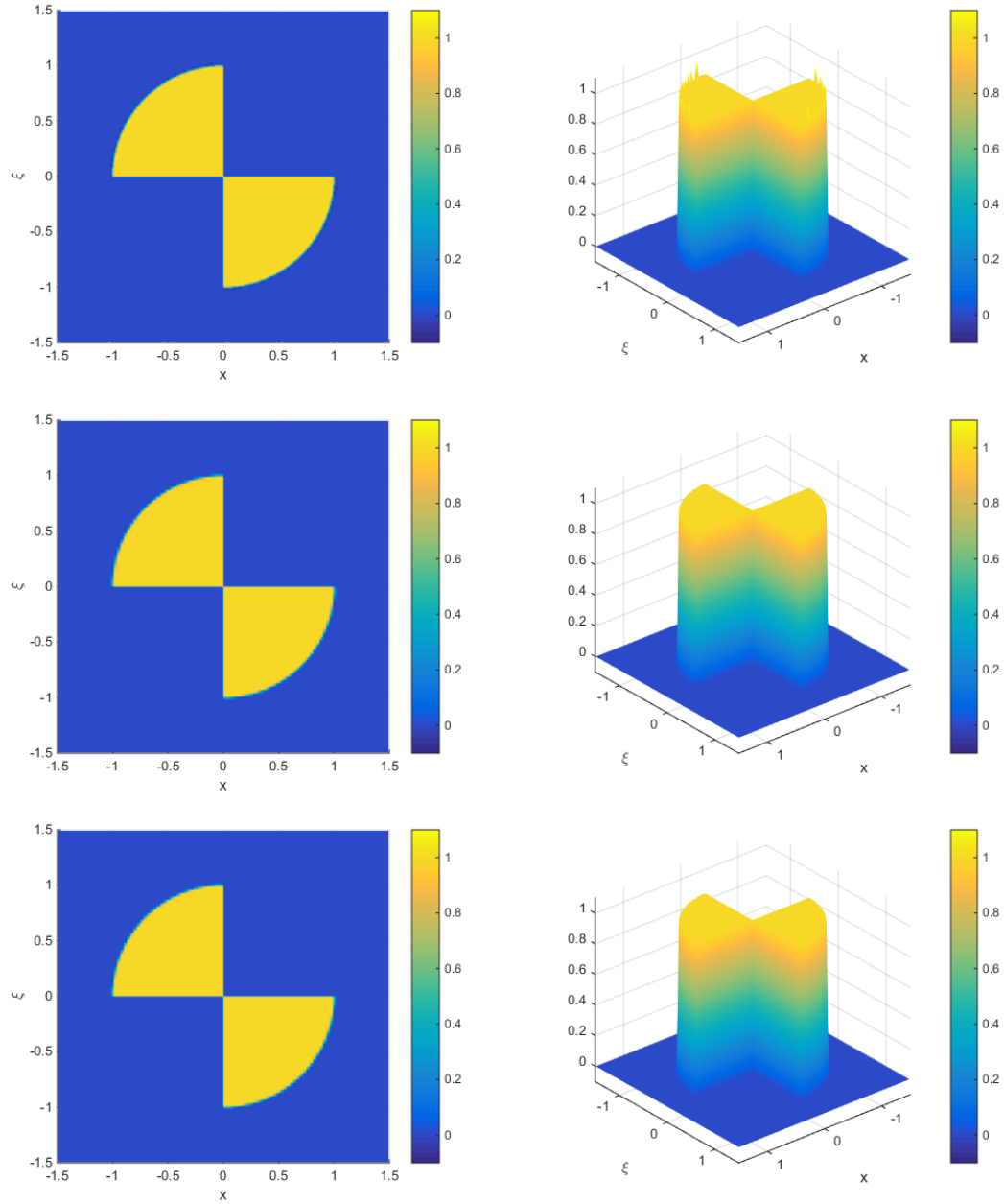


FIG. 5.1. 1D1V problem with an exact L^∞ solution in Example 5.2. Contour plot (left) and 3D plot (right) of the initial solution at $t = 0$ without limiter (top), initial solution after applying the TVB minmod limiter (middle), and initial solution after applying the bound-preserving limiter (bottom) on 100×100 meshes.

437 where

$$438 \quad (5.6) \quad \nu(x) = \begin{cases} 0.9, & x \leq -2, \\ 0.9 - \frac{0.9}{4}(x+2)^2, & -2 < x \leq 0, \\ -0.9 + \frac{0.9}{4}(x-2)^2, & 0 < x < 2, \\ -0.9, & x \geq 2. \end{cases}$$

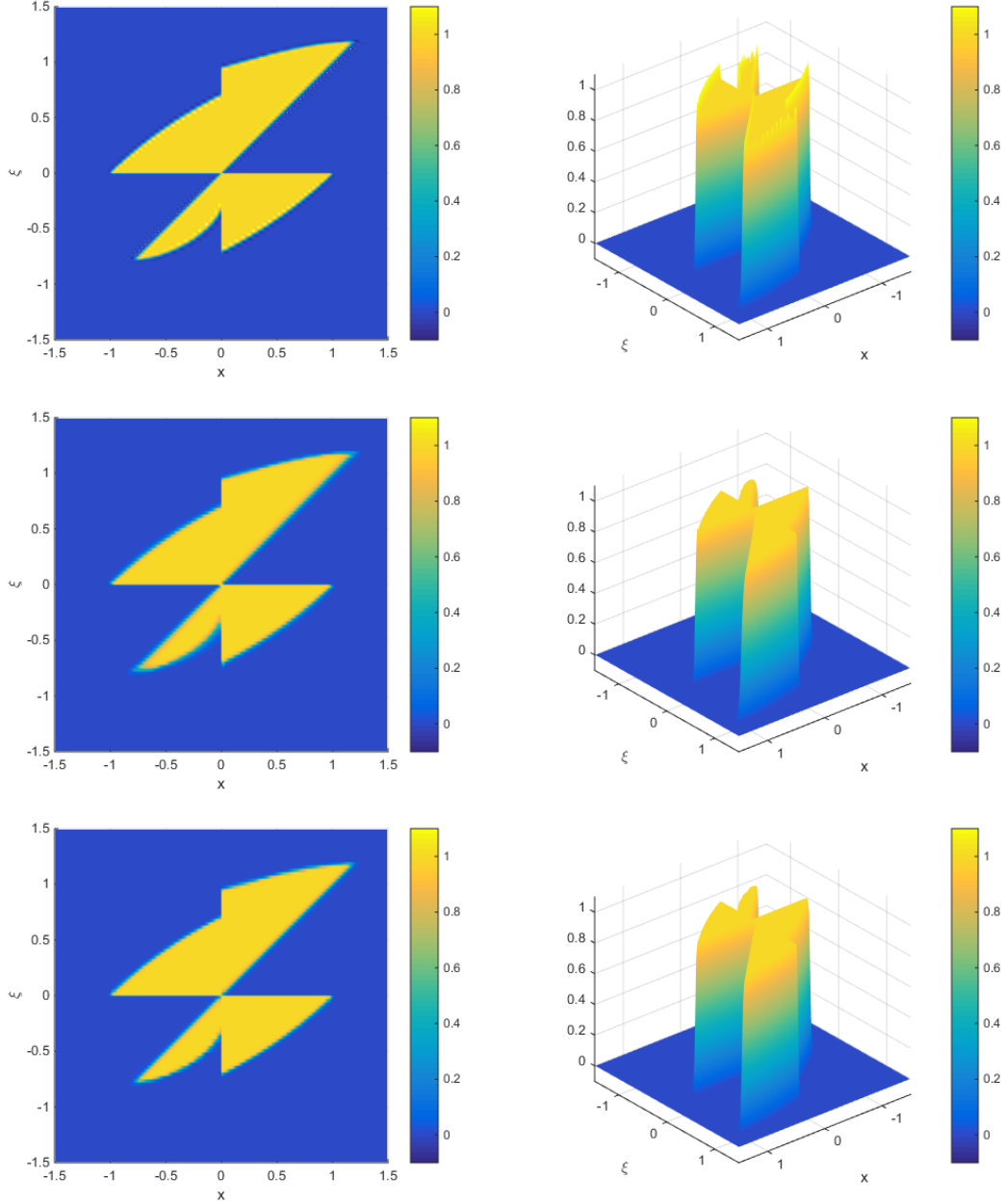


FIG. 5.2. 1D1V problem with an exact L^∞ solution in Example 5.2. Contour plot (left) and 3D plot (right) of the numerical solution of DG method without any limiter (top), numerical solution of DG method with the TVB minmod limiter (middle) and numerical solution of the proposed DG method with the bound-preserving limiter (bottom) on 100×100 meshes at $t = 1$ (with $k = 2$).

The computational domain is $[-2, 2] \times [-1.6, 1.6]$. This example is a 1D1V problem with a measure-valued solution [19], which may arise in the computation of the semiclassical limit of the Schrodinger equation. We are interested in the approximation of the moments, such as the density ρ and the averaged velocity u , defined

as

$$\rho(x, t) = \int f(x, \xi, t) d\xi, \quad u(x, t) = \frac{\int f(x, \xi, t) \xi d\xi}{\int f(x, \xi, t) d\xi}.$$

Following the level set method proposed in [18] for smooth potentials and extended in [19] to discontinuous potentials, we decompose f into the level set function f_1 and the modified density function f_2 , which satisfy the same Liouville equation (2.1) with the following initial conditions

$$f_1(x, \xi, 0) = 1, \quad f_2(x, \xi, 0) = \xi - \nu(x).$$

439 The moments ρ and u can be numerically approximated by

$$\begin{aligned} 440 \quad (5.7) \quad \rho(x, t) &= \int f_1(x, \xi, t) \delta_\omega(f_2(x, \xi, t)) d\xi, \\ 441 \quad u(x, t) &= \frac{1}{\rho(x, t)} \int f_1(x, \xi, t) \xi \delta_\omega(f_2(x, \xi, t)) d\xi, \end{aligned}$$

442 on a uniform mesh [14]. Here δ_ω is an approximation to the δ function, given by

$$443 \quad (5.8) \quad \delta_\omega(x) = \begin{cases} \frac{1}{2\omega}(1 + \cos(|\pi x|/\omega)), & \left| \frac{x}{\omega} \right| \leq 1, \\ 0, & \left| \frac{x}{\omega} \right| > 1, \end{cases}$$

and ω is taken as half of the support size of the discrete delta function δ_ω . In our computation, we take

$$\omega = \max(|(f_2)_\xi|, 1) \Delta x,$$

445 where the derivative $(f_2)_\xi$ can be directly computed from the polynomial expression of f_2 in each cell. The
446 exact velocity profile and the corresponding velocity at $t = 1.8$ can be found in the Appendix of [19].

447 We perform numerical simulations for the proposed DG method with P^2 piecewise polynomials on 400×320
448 meshes up to $t = 1.8$. Figures 5.3 shows the density and the averaged velocity of the exact solutions and
449 numerical solutions at $t = 1.8$. The numerical solutions are obtained by the HPDG method with the TVB
450 minmod limiter [10], and by the HPDG method with the bound-preserving limiter to keep $-2.4 \leq f_2 \leq 2.4$
451 for the decomposed equation $f_2(x, \xi, 0) = \xi - \nu(x)$. We observe that both limiters can achieve satisfying
452 non-oscillatory results for the density, while the boundary-preserving limiter yields a better non-oscillatory
453 approximation than the TVB minmod limiter for the averaged velocity, especially in the average velocity plot
454 near the region $x \in [0.3, 1]$. In addition, we also observe that the average velocity is better resolved in this
455 region when compared with the result in [19] obtained with the finite volume method on a much refined mesh,
456 thanks to the high order feature of the proposed HPDG methods.

457 *Example 5.4. 2D2V problem with a measure-valued solution*

458 In this example, we consider two-dimensional Liouville equation given by

$$459 \quad (5.9) \quad f_t + \xi f_x + \eta f_y - V_x f_\xi - V_y f_\eta = 0,$$

461 with a discontinuous potential

$$462 \quad (5.10) \quad V(x, y) = \begin{cases} 0.1, & x > 0, y > 0, \\ 0, & \text{else.} \end{cases}$$

464 The initial condition takes the form

$$465 \quad (5.11) \quad f(x, y, \xi, \eta, 0) = \rho(x, y, 0) \delta(\xi - p(x, y)) \delta(\eta - q(x, y)),$$

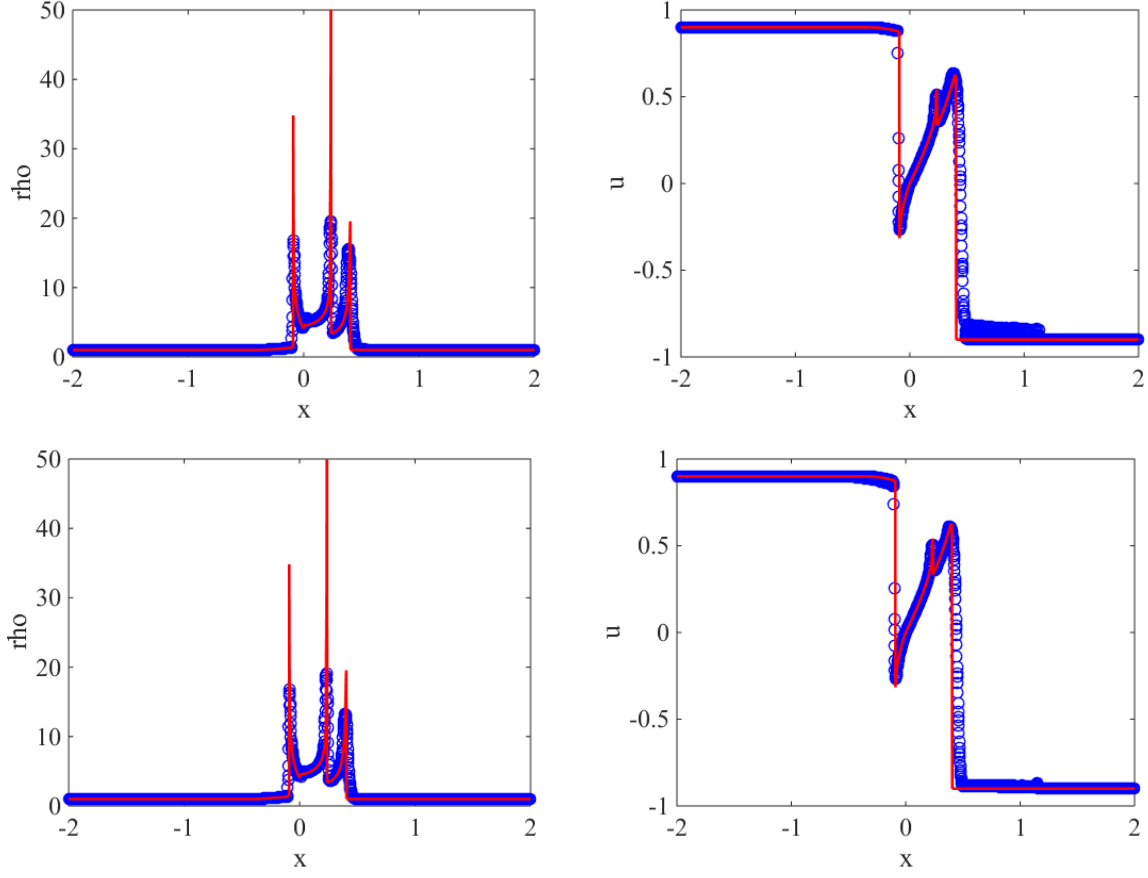


FIG. 5.3. 1D1V problem with a measure-valued solution in Example 5.3. Exact solution (lines) and numerical solution (circles) of the density (left) and the averaged velocity (right) of the proposed DG method at $t = 1.8$ with $k = 2$ using the TVB minmod limiter (top) and the bound-preserving limiter (bottom), on 400×320 meshes.

467 where

$$468 \quad (5.12) \quad \rho(x, y, 0) = \begin{cases} 0, & x > -0.1, y > -0.1, \\ 1, & \text{else,} \end{cases}$$

$$469 \quad (5.13) \quad p(x, y) = q(x, y) = \begin{cases} 0.4, & x > 0, y > 0, \\ 0.6, & \text{else.} \end{cases}$$

470

471 The computational domain is set as $[x, y, \xi, \eta] \in [-0.2, 0.2] \times [-0.2, 0.2] \times [0.3, 0.9] \times [0.3, 0.9]$. This example is
 472 a 2D2V problem with a measure-valued solution studied in [19]. We are interested in the approximation of the
 473 zeroth moment, i.e. the density ρ , defined as

$$474 \quad (5.14) \quad \rho(x, y, t) = \int \int f(x, y, \xi, \eta, t) d\xi d\eta.$$

475

476 The exact density at time $t = 0.4$ is given by

$$477 \quad (5.15) \quad \rho(x, y, 0.4) = \begin{cases} 1, & x < 0 \text{ or } y < 0, \\ 1.5, & 0 \leq x \leq \frac{14}{150}, \quad y \geq \frac{3x}{2}, \\ 1.5, & 0 \leq y \leq \frac{14}{150}, \quad y \leq \frac{2x}{3}, \\ 0, & \text{otherwise.} \end{cases}$$

478
 479 We perform numerical simulations of the proposed HPDG method with piecewise P^1 polynomials up to
 480 $t = 0.4$ with a positivity-preserving limiter. Figure 5.4 shows numerical results of the density ρ with 12^4 , 20^4
 481 and 30^4 meshes in the phase space, compared with the reference exact solution. We can observe that as the
 482 meshes are refined, the solution converges to the exact solution. When compared with the numerical results in
 483 [19], the proposed high order HPDG method can achieve a sharper transition near discontinuity with a coarser
 484 mesh.

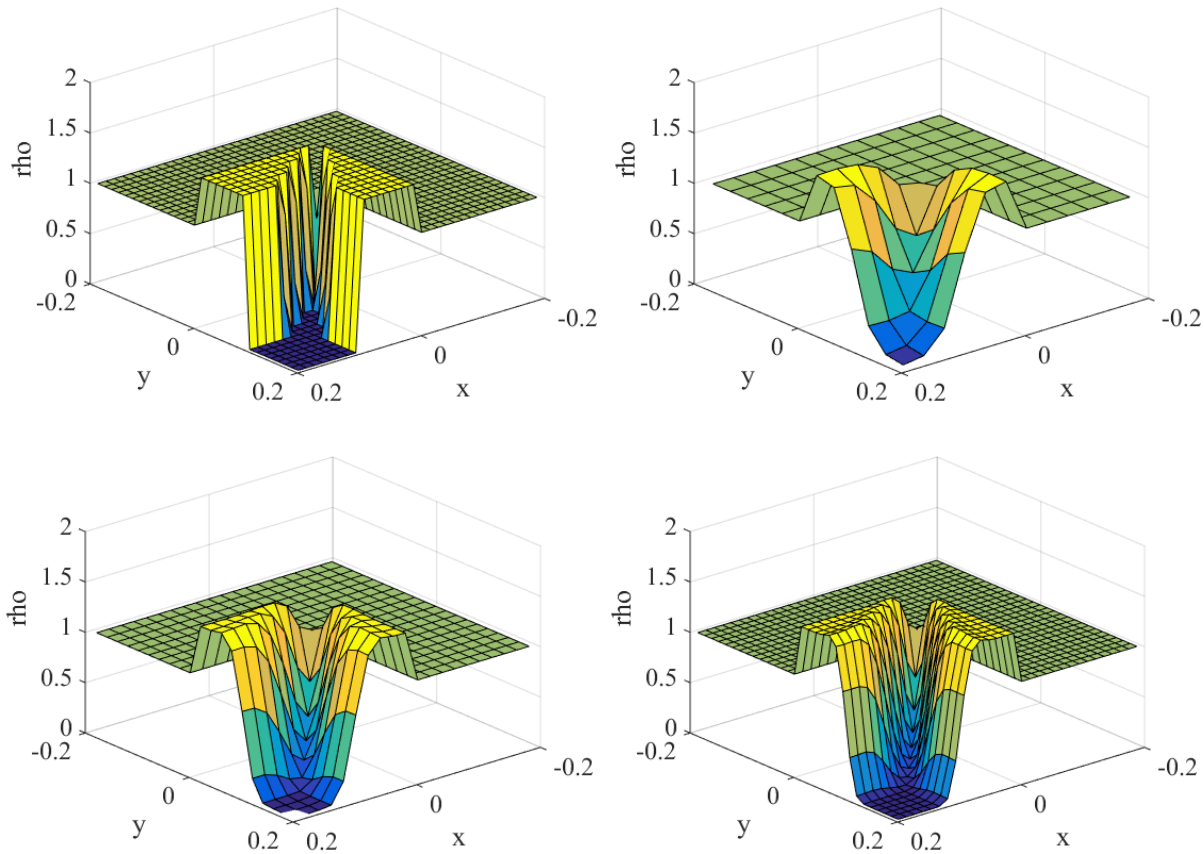


FIG. 5.4. $2D2V$ problem with a measure-valued solution in Example 5.4. Exact solution (top left) and numerical solutions of the density with $k = 1$ on the 12^4 (top right), 20^4 (bottom left) and 30^4 (bottom right) meshes at $t = 0.4$.

485 **6. Conclusions.** In this paper, we design the HPDG method for the Liouville equation with discontinuous
 486 potentials, to maintain constant Hamiltonian across a potential barrier, which allows to capture the correct
 487 transmission and reflection behavior of particles. The proposed method can also be viewed as a high order
 488 extension of the finite difference and finite volume methods discussed in [19]. Based on the standard DG

method for hyperbolic conservation laws, we make extra effort to construct numerical fluxes to take care of the behavior of a particle at a potential barrier such as either crossing it with a different momentum or being reflected. We further apply a positivity-preserving limiter to add extra robustness and stability. We provide a theoretical study of the positivity and stability properties of our proposed scheme. Numerical results show the accuracy and robustness of the proposed methods for 1D1V and 2D2V test problems. The discontinuity of the potential $V(x)$ in the 2D2V setting is assumed to occur only in the direction aligned with our spatial discretization in this paper. Future works include the generalization of the HPDG scheme to the case of curved discontinuity to further leverage the flexibility of DG method, and the study of HPDG method on unstructured meshes to accommodate general computational domains.

Acknowledgements. S. Jin was partially supported by NSFC grant No. 12031013 and by Innovation Program of Shanghai Municipal Education Commission (No. 2021-01-07-00-02-E0087). Y. Xing was partially supported by the NSF grant DMS-1753581. X. Zhong was partially supported by NSFC Grant No. 11871428.

501

REFERENCES

- 502 [1] Ambrosio, Luigi Transport equation and Cauchy problem for BV vector fields. *Invent. Math.*, 2(158):227–260, 2004.
 503 [2] F. Bouchut and F. James. One-dimensional transport equations with discontinuous coefficients. *Nonlinear Analysis, Theory, Methods and Applications*, 32:891–933, 1998.
 504 [3] I. Capuzzo Dolceta and B. Perthame. On some analogy between different approaches to first order PDEs with non-smooth coefficients. *Adv. Math. Sci. Appl.*, 6:689–703, 1996.
 505 [4] Y. Cheng, A. J. Christlieb, and X. Zhong. Energy-conserving discontinuous Galerkin methods for the Vlasov–Ampère system. *Journal of Computational Physics*, 256:630–655, 2014.
 506 [5] Y. Cheng, A. J. Christlieb, and X. Zhong. Energy-conserving discontinuous Galerkin methods for the Vlasov–Maxwell system. *Journal of Computational Physics*, 279:145–173, 2014.
 507 [6] Y. Cheng, I.M. Gamba, A. Majorana and C.-W. Shu, A brief survey of the discontinuous Galerkin method for the Boltzmann–Poisson equations, *SEMA Journal*, 54, 47–64, 2011.
 508 [7] B. Cockburn, S. Hou and C.-W. Shu. The Runge-Kutta local projection discontinuous Galerkin finite element method for conservation laws IV: the multidimensional case, *Mathematics of Computation*, 54, 545–581, 1990.
 509 [8] B. Cockburn, G. Karniadakis and C.-W. Shu. The development of discontinuous galerkin methods. In B. Cockburn, G. Karniadakis, and C.-W. Shu, editors, *Discontinuous Galerkin Methods: Theory, Computation and Applications*, pages 3–50. Lecture Notes in Computational Science and Engineering, Part I: Overview, volume 11, Springer, 2000.
 510 [9] B. Cockburn, S.-Y. Lin and C.-W. Shu, TVB Runge-Kutta local projection discontinuous Galerkin finite element method for conservation laws III: one dimensional systems, *Journal of Computational Physics*, 84, 90–113, 1989.
 511 [10] B. Cockburn and C.-W. Shu. TVB Runge–Kutta local projection discontinuous Galerkin finite element method for conservation laws II: General framework. *Mathematics of Computation*, 52(186):411–411, 1989.
 512 [11] B. Cockburn and C.-W. Shu. Runge–Kutta discontinuous Galerkin methods for convection-dominated problems. *Journal of Scientific Computing*, 16(3):173–261, 2001.
 513 [12] R. J. DiPerna and P. L. Lions. Ordinary differential equations, transport theory and Sobolev spaces. *Invent. Math.*, 98(3):511–547, 1989.
 514 [13] E. Endeve, C.D. Hauck, Y. Xing and A. Mezzacappa, Bound-preserving discontinuous Galerkin methods for conservative phase space advection in curvilinear coordinates, *Journal of Computational Physics*, 287, 151–183, 2015.
 515 [14] B. Engquist, A.-K. Tornberg, and R. Tsai. Discretization of Dirac delta functions in level set methods. *Journal of Computational Physics*, 207(1):28–51, 2005.
 516 [15] F. Filbet and C.-W. Shu, Discontinuous-Galerkin methods for a kinetic model of self-organized dynamics potentials, *Mathematical Models and Methods in Applied Sciences (M³AS)*, 28, 1171–1197, 2018.
 517 [16] L. Gosse and F. James. Numerical approximations of one-dimensional linear conservation equations with discontinuous coefficients. *Math. Comp.*, 69:987–1015, 2000.
 518 [17] S. Jin and X. Liao. A Hamiltonian-preserving scheme for high frequency elastic waves in heterogeneous media. *Journal of Hypobolic Differential Equations*, 3(4):741–777, 2006.
 519 [18] S. Jin, H. Liu, S. Osher, and Y.-H. R. Tsai. Computing multivalued physical observables for the semiclassical limit of the Schrödinger equation. *Journal of Computational Physics*, 205(1):222–241, 2005.
 520 [19] S. Jin and X. Wen. Hamiltonian-preserving schemes for the Liouville equation with discontinuous potentials. *Comm. Math. Sci.*, 3(3):285–315, 2005.
 521 [20] S. Jin and X. Wen. Hamiltonian-preserving schemes for the Liouville equation of geometrical optics with discontinuous local wave speeds. *Journal of Computational Physics*, 214:672–697, 2006.
 522 [21] S. Jin and X. Wen. A Hamiltonian-preserving scheme for the Liouville equation of geometrical optics with partial transmissions and reflections. *SIAM Journal on Numerical Analysis*, 44:1801–1828, 2006.
 523 [22] S. Jin and D. Yin. Computational high frequency waves through curved interfaces via the Liouville equation and geometric theory of diffraction. *Journal of Computational Physics*, 227(12):6106–6139, 2008.
 524 [23] X. Li. l^1 -error estimates for a Hamiltonian-preserving Liouville equation the Liouville equation with piecewise constant

546

- 547 potentials: a simple proof. *Journal of Computational Mathematics*, 35(6):814–827, 2017.
- 548 [24] X. Liu and S. Osher. Nonoscillatory high order accurate self-similar maximum principle satisfying shock capturing schemes
549 I. *SIAM Journal on Numerical Analysis*, 33(2):760–779, 1996.
- 550 [25] B. Perthame and C.-W. Shu. On positivity preserving finite volume schemes for Euler equations. *Numerische Mathematik*,
551 73(1):119–130, 1996.
- 552 [26] B. Perthame and C. Simeoni. A kinetic scheme for the Saint-Venant system with a source term. *Calcolo*, 38:201–231, 2001.
- 553 [27] G. Petrova and B. Popov. Linear transport equations with discontinuous coefficients. *J. Math. Anal. Appl.*, 260:307–324.
554 2001.
- 555 [28] F. Poupaud and M. Rasclé. Measure solutions to the linear multidimensional transport equation with non-smooth coefficients.
556 *Comm. PDEs*, 22:337–358. 1997.
- 557 [29] J.-M. Qiu and C.-W. Shu, Positivity preserving semi-Lagrangian discontinuous Galerkin formulation: theoretical analysis
558 and application to the Vlasov-Poisson system, *Journal of Computational Physics*, 230, 8386–8409, 2011.
- 559 [30] W.H. Reed and T. Hill, *Triangular mesh methods for the neutron transport equation*, Technical report, Los Alamos Scientific
560 Lab., N. Mex. (USA), 1973.
- 561 [31] C.-W. Shu and S. Osher. Efficient implementation of essentially non-oscillatory shock-capturing schemes. *Journal of Com-
562 putational Physics*, 77(2):439–471, 1988.
- 563 [32] J. Staudacher and E. Savin. Conservative finite-difference scheme for high-frequency acoustic waves propagating at an
564 interface between two media. *Commun. Comput. Phys.*, 11(2):351–366, 2012.
- 565 [33] X. Wen. The l^1 -error estimates for a Hamiltonian-preserving Liouville equation the Liouville equation with piecewise constant
566 potentials and perturbed initial data. *Journal of Computational Mathematics*, 29(1):1–23, 2010.
- 567 [34] X. Wen and S. Jin. The l^1 -error estimates for a Hamiltonian-preserving scheme for the Liouville equation with piecewise
568 constant potentials. *SIAM Journal on Numerical Analysis*, 46:2688–2714, 2008.
- 569 [35] X. Wen and S. Jin. The l^1 -stability of a Hamiltonian-preserving Liouville equation the Liouville equation with discontinuous
570 potentials. *Journal of Computational Physics*, 27(1):45–67, 2009.
- 571 [36] X. Zhang and C.-W. Shu. Maximum-principle-satisfying and positivity-preserving high-order schemes for conservation laws:
572 survey and new developments. *Proceedings of the Royal Society A: Mathematical, Physical and Engineering Sciences*,
573 467(2134):2752–2776, 2011.
- 574 [37] X. Zhang and C. Shu. On positivity preserving high order discontinuous Galerkin schemes for compressible Euler equations
575 on rectangular meshes. *Journal of Computational Physics*, 328:301–343, 2017.